# RADARSAT SCANSAR WIND RETRIEVAL AND RAIN EFFECTS ON SCANSAR MEASUREMENTS UNDER HURRICANE CONDITIONS

*Congling Nie and David G. Long*

Electrical and Computer Engineering Department
Brigham Young University, 459 CB, Provo, Utah 84602

**ABSTRACT**

RADARSAT-1 ScanSAR SWA images of Hurricane Katrina are used to retrieve surface wind vectors over the ocean. Collocated H*wind wind directions are used as the wind direction while the wind speed is derived from SAR $\sigma^\circ$ by inversion of a C-band HH-polarization Geophysical Model Function (GMF) that is derived from the VV-polarization GMF, CMOD5, using a polarization ratio model. Because existing polarization models do not fit the ScanSAR SWA data well, a recalibration model is proposed to "recalibrate" the ScanSAR SWA images. Validated with collocated H*wind wind speed estimates, the mean difference between SAR-retrieved and H*wind speed is small and the root mean square (RMS) error is below 4 m/s. Rain effects on the ScanSAR measurements are analyzed for an incidence angle range of $22^\circ$ to $23.6^\circ$ using collocated ground-based Doppler weather radar (NEXRAD) rain measurements.

## 1. INTRODUCTION

Recent studies confirm that C-band SAR measurements can be used in the retrieval of the near-ocean surface winds at high resolution [1]. Similar to scatterometry, the normalized radar cross section ($\sigma^\circ$) measured by SAR over the ocean is mainly from wind-driven gravity-capillary waves (Bragg waves). Since SAR has only one measurement for each geographic location, wind speed and direction can not be simultaneously retrieved by direct inversion of the GMF, which is the general method of scatterometry. The wind direction must be estimated by measuring the orientation of wind-induced streaks visible in most SAR images [1, 2], or obtained from additional information such as numerical wind prediction. For SAR wind speed retrieval, there are two main methods: estimation of wind speed from the spectral width of the image spectrum in azimuth direction, or inversion of the GMF from the measured $\sigma^\circ$.

The Canadian satellite RADARSAT-1 operates at 5.3 GHz in HH-polarization. The scanning SAR (ScanSAR) wide A (SWA) mode of RADARSAT-1 provides coverage of a 500km nominal ground swath at incidence angles between 20 and 49 degrees, with a spatial resolution of 100 m [3]. Because ScanSAR SWA's resolution is insufficient to implement the spectrum method for extracting wind direction from surface featues, the wind direction must be inferred from a numerical model. The wind speed can be estimated by inversion of the GMF. Unfortunately, there is no well-validated GMF model for HH-polarization at C-band. Our general approach to obtain an HH-polarization GMF is to adjust the C-band VV-polarization GMF (CMOD) using a polarization ratio $p$. While several C-band polarization ratio models have been proposed, none have been well verified in hurricane conditions.

Although C-band backscatter has been generally believed to be little affected by rain, rain cells are often observed on C-band SAR images over the ocean [4] [5]. Rain-induced backscatter is from atmospheric attenuation and scattering by falling rain drops and from rain-induced surface scattering on the ocean surface. In the past, several investigations have been performed to analyze SAR signatures of rain cells over the ocean. Melshimer et al. showed that rain generally damps the surface backscatter at low incidence angles and enhances the backscatter at high incidence angles [4]. Nie and Long [6] found that rain surface backscatter can dominate the total backscatter from the ocean surface acquired by C-band radar in moderate to heavy rains by studying the rain effects on ESCAT scatterometer measurements.

In this study, we develop a "recalibration" model for ScanSAR SWA data and demonstrate that relatively reliable estimates of wind speed can be obtained in hurricanes using SAR measurements. Rain effects on ScanSAR SWA data are then examined with the aid of collocated shore-based NEXRAD weather radar data. In this study we use images of Hurricane Katrina (August 2005).

## 2. SAR WIND RETRIEVAL

As mentioned, additional information such as numerically predicted wind fields must be used to estimate the wind direction. In this study, the collocated H*wind direction field is used as the wind direction for SAR wind retrieval. Knowing the wind direction, the wind speed can be derived from the $\sigma^\circ$ image by inversion of the GMF using the incidence angle $\theta$, the radar azimuth angle, and the wind direction. Lacking a well-validated GMF for C-band HH-polarization, the GMF for C-band VV-polarization is modified using the C-band polarization ratio to estimate the $\sigma^\circ$.

Several C-band polarization models have been proposed using different data sets [7, 8]. Because the polarization models are not well-validated and the model coefficients have a dependency on the specific data set, we compare different models using our data. The $\sigma^\circ$ estimates from SAR image DN values are compared with the $\sigma^\circ$ computed from H*wind wind estimates projected through the scatterometer CMOD5 GMF and the polarization model. I reasonable fit is found using the Thompson et al. [7] model for the polarization ratio

$$p = \frac{(1 + \alpha \tan^2 \theta)^2}{(1 + 2\tan^2 \theta)^2} \tag{1}$$

where $\theta$ is the incidence angle, and $\alpha$ is a constant. The polarization model fits SWA image A relatively well for $\alpha = 0.6$. The fit to image B is not as good. However, image B was acquired over the transition between land and ocean, which may have impacted the calibration.

To compensate for the limitations of calibration and the polarization ratio model, we adopt a backscatter adjustment model proposed

**Table 1**. Coefficients of the recalibration model.

| Image | incidence angle (deg) | n | M | O |
|---|---|---|---|---|
| A | 22 - 31 | -1.12 | 0.34 | 0.032 |
| B | 22 - 31 | -1.7 | 0.22 | 0.002 |
| A | 31 - 41 | -1.2 | 0.32 | 0.01 |
| B | 31 - 41 | -1.18 | 0.27 | 0.008 |
| A | 41 - 47 | -1.11 | 0.33 | 0.003 |
| B | 41 - 47 | -1.115 | 0.33 | 0.0055 |

in [9] to recalibrate the SAR measurements. The calibration model coefficients are "tuned" for optimum performance using collocated H*wind wind fields projected through CMOD5 and Thompson's polarization model.

The re-calibrated $\sigma^{\circ}_{re}$ can be expressed as

$$\sigma^{\circ}_{re} = \sigma^{\circ}_{es} G(\theta) M + O \tag{2}$$

where $\sigma^{\circ}_{es}$ is the $\sigma^{\circ}$ estimate from DN value using Eq. (1), $G(\theta)$ is a parameter dependent on incidence angle, M is a power correction parameter, and $O$ is an offset correction parameter. $G(\theta)$ can be expressed as

$$G(\theta) = \sin^{n}(\theta) \tag{3}$$

where $n$ is a real number. Since ScanSAR SWA combines data from four different beams, each with different incidence angles and different radiometric characteristics, the coefficients of the recalibration model are separately "tuned" for different incidence angle ranges. Table 1 shows the recalibration coefficients of image A and B for three incidence angle bins of 22-31 degrees, 31-41 degrees, and 41-47 degrees, respectively. It is noted that except for the incidence angle range 22-31 degrees, the coefficients of the recalibration model are very similar for each case, showing the recalibration model is consistent for different SAR image segments.

## 3. WIND RETRIEVAL RESULTS AND ANALYSIS

Based on the recalibation model, wind retrieval is done at 1 km $\times$ 1 km by inversion of the GMF using recalibrated $\sigma^{\circ}$. To validate the SAR-derived wind speeds, we show scatter density plots between the SAR retrieved wind speed fields and the collocated H*wind wind speed fields for image A in Fig. 1. Overall, SAR-derived wind speeds agree well with H*wind wind speeds. Except for the influence of rain, the largest errors of wind speed occur at high wind speed (over 25 m/s), where the SAR-derived wind speeds have considerable scatter in comparison to the H*wind wind speeds. These errors are mainly due to the saturation of the C-band GMF CMOD5. Another reason may be inaccuracy of CMOD5 at high wind speed.

The mean error (SAR retrieved wind - H*wind wind) and RMS error between the two wind speed estimates are listed in Table 2. The ScanSAR SWA retrieved wind speed has a small bias, which is possibly caused by rain contamination. The overall RMS error is below 6 m/s, and the RMS error for wind speeds less than 25 m/s is below 4 m/s, demonstrating relatively high accuracy of SAR-retrieved wind speeds in hurricanes.

## 4. WIND/RAIN BACKSCATTER MODEL FOR SAR

In raining areas, the SAR-measured normalized radar cross section over the ocean is affected by rain atmospheric effects and various

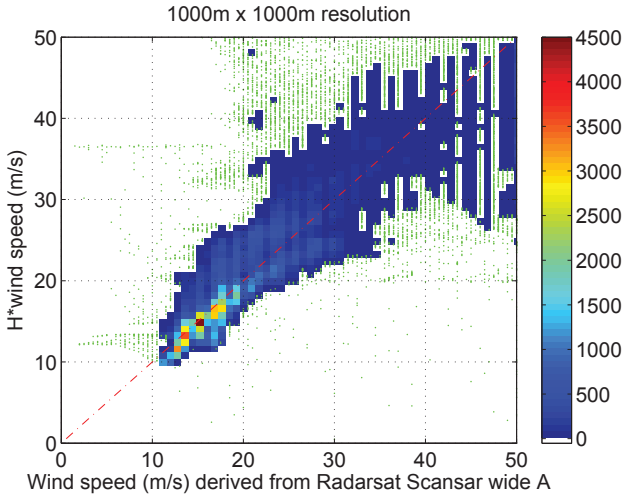


**Fig. 1**. Scatter density plot for the SAR-derived wind speed and H*wind speed for SAR image A in m/s.

**Table 2**. Mean and RMS errors in m/s between the SAR-retrieved and H*wind speeds.

| Image | Mean | RMS (overall) | RMS (<25 m/s) |
|---|---|---|---|
| A | -0.21 | 4.53 | 2.5 |
| B | 0.38 | 5.7 | 3.5 |

surface effects including splash products, turbulence, and downdraft. Furthermore, the effect of surface turbulence varies with the temporal evolution of the rain event. At the beginning of the rain event, the wave damping effect induced by rain is insignificant because surface turbulence is under development. The damping grows during the rain event then decays after the rain moves on. Since the turbulence decays slowly due to the molecular viscosity of water and the length scales of the turbulence, the damping effect can exist for some time after a rain event ends [4]. Unfortunately, the lifetime of rain-induced turbulence in water has rarely been studied. As a reference, the lifetime of votex rings generated by rain drops impinging the water surface is of the order of a minute for a drop diameter of 1 mm [10]. In the analysis of the SAR measurements, the damping effect is still observed about five minutes after rain events. Therefore, it is assumed that the lifetime of rain-induced surface turbulence is of the order of several minutes.

Here, we model the bulk effect of rain on the Bragg wave field in the rain core area by combining all the surface contributions together into a single rain surface perturbation term, $\sigma_{surf}$. $\sigma_{surf}$ is assumed to be additive with the wind-induced surface backscatter. The rain-modified measured backscatter, $\sigma_m$, is represented by a simple additive model

$$\sigma_m = (\sigma_{wind} + \sigma_{surf})\alpha_{atm} + \sigma_{atm} \tag{4}$$

where $\sigma_{wind}$ is the wind-induced surface backscatter, $\sigma_{surf}$ is the rain-induced surface perturbation backscatter, $\alpha_{atm}$ is the two-way rain-induced atmospheric attenuation, and $\sigma_{atm}$ is rain-induced atmospheric backscatter.

### 4.1. Evaluation of Atmospheric Attenuation and Backscattering

The SAR measurement geometry is displayed in Fig. 2. For simplicity, we use a plane-wave incidence approximation to represent the

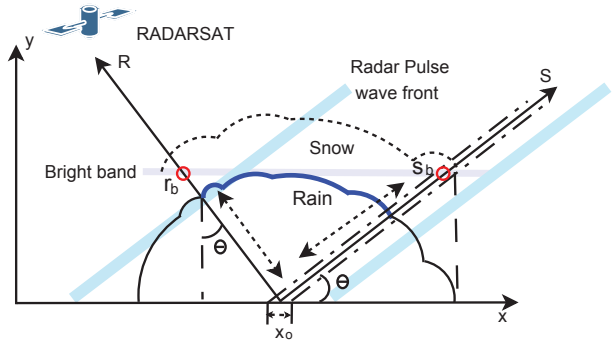


**Fig. 2**. Schematic diagram of the SAR scattering geometry for a rain cell. The oblique lines represent the radar pulse under the approximation of plane wave incidence.

synthetic aperture radar pulse. We define a new coordinate system $r - s$. $r$ is along the SAR slant range and $s$ is perpendicular to $r$. For the SAR surface backscatter at $x_\circ$, the atmospheric attenuation is contributed by the raindrops along coordinate $r$ from the surface to the bright band altitude and by snow above the bright band. The typical altitude of the bright band is about 5 km.

The attenuation coefficient of rain, $K_r$, can be estimated using the $K_r$–$R$ ($R$ is rain rate in mm/hr) relationship [11]. The path-integrated attenuation (PIA) in dB is equal to the integration of $K_r(r, s)$ through the $R$ axis ($s = 0$), from the bright band altitude $r_b$ (shown in Fig. 2), to the ocean surface 0,

$$PIA = 2 \int_0^{r_b} k_r(r, 0) dr \quad \text{dB} \tag{5}$$

where $k_r(r, 0) = aR(r, 0)^b$. The two-way atmospheric attenuation factor $\alpha_{atm}$ is calculated by converting the PIA to normal space. The atmospheric backscatter ($\sigma_{atm}$) observed by the SAR is estimated from the rain rate using a similar method that is decribed in detail in [12].

After calculating $\sigma_{atm}$ and $\alpha_{atm}$, we estimate the surface perturbation backscatter $\sigma_{surf}$ by

$$\sigma_{surf} = \alpha_{atm}^{-1}(\sigma_m - \sigma_{atm}) - \sigma_{wind} \tag{6}$$

where the $\sigma_{surf}$ can be negative at low incidence angles, corresponding to the loss of the wind-induced backscatter. A positive value is an increase in the net backscatter.

We analyze the radar backscatter of a particular rain cell at incidence angles between 22° and 23.6°. At this incidence angle, the dominant rain effect is a damping of the the surface backscatter; hence, the rain cell looks darker than the surrounding rain-free ocean in the SAR image. The H*wind model predicts that the wind speed in this area is essentially constant. Radar data from LIX NEXRAD station is used to calculate the rain rates.

Figure 3(a) and (b) display the collocated $\sigma_{surf}$ and the NEXRAD surface rain rate, respectively. In Fig. 3(c) and (d), the profiles of rain rate and $\sigma^\circ_{surf}$ are plotted along the red solid line in Fig. 3(a) and (b). These show that the $\sigma^\circ_{surf}$ generally decreases as rain rate increases. Note that the profile of $\sigma^\circ_{surf}$ is wider than the rain rate profile.

To relate the $\sigma_{surf}$ with rain rate, we use a power law model [6]. Because the estimate of $\sigma_{surf}$ is relatively noisy, we first make a nonparametric estimate of $\sigma_{surf}$ as a function of $R_{\text{dB}}$ using an

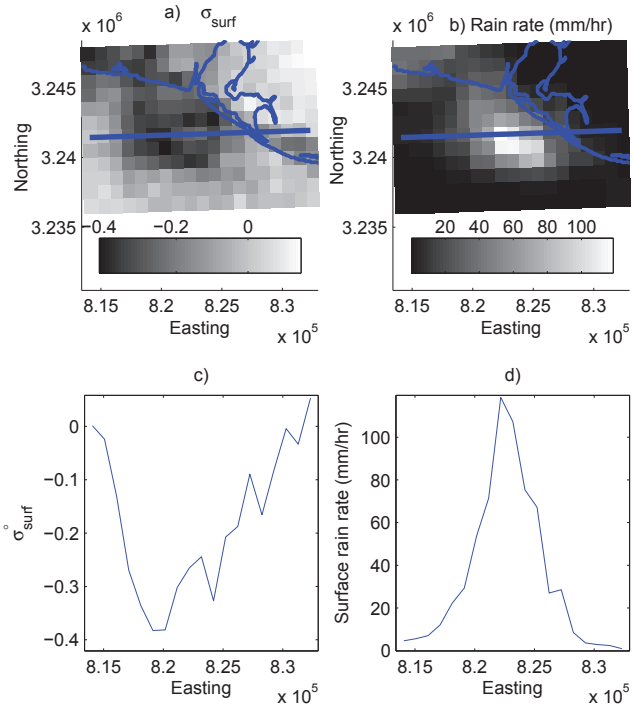


**Fig. 3**. (a) $\sigma^\circ_{surf}$ of a particular rain cell. (b) Collocated NEXRAD rain rate in mm/hr. (c) and (d) Profile of $\sigma^\circ$ and rain rate along the solid line plotted in (a) and (b).

Epanechnikov kernel with a 2 mm/hr dB bandwidth in rain rate as shown in Fig. 4(a). Then, we estimate the model coefficients for the quadratic model using a linear least-squares fit.

## 5. CONCLUSION

RADARSAT-1 ScanSAR SWA images of Hurricane Katrina are used to retrieve surface wind vectors over the ocean. Collocated H*wind wind directions are used as the wind direction estimate and the wind speed is derived from SAR $\sigma^\circ$ by inversion of a C-band HH-polarization GMF that is derived from the VV-polarization CMOD5 GMF, using a polarization ratio model. Because existing polarization models do not fit the ScanSAR SWA data well, a recalibration model is proposed to "recalibrate" the ScanSAR SWA images. Validated with collocated H*wind wind speed estimates, the mean difference between SAR-retrieved and H*wind speed is small and the RMS error is below 4 m/s. Rain effects on the ScanSAR measurements are analyzed for incidence angle range $22^\circ - 23.6^\circ$ using collocated ground-based Doppler weather radar (NEXRAD) rain measurements.

## 6. REFERENCES

[1] C. C. Wackerman, C. L. Rufenach, R. Schuchman, J. A. Johnnessen, and K. Davidson, "Wind vector retrieval using ERS-1 synthetic aperture radar imagery," *Journal of Geophysical Research*, vol. 34, pp. 1343–1352, 1996.

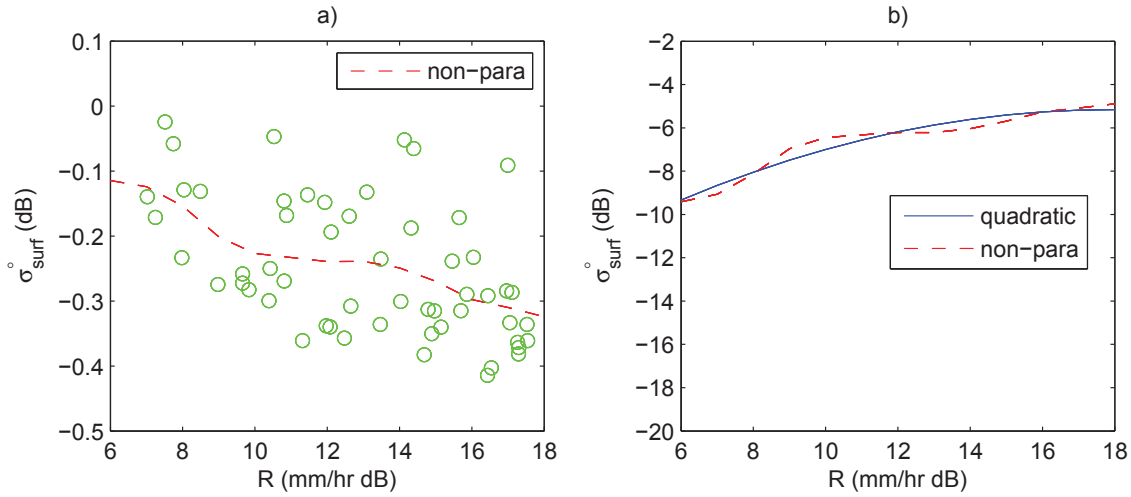


**Fig. 4**. (a) $\sigma^{\circ}_{surf}$ versus rain rate nonparametric fit. (b) Quadratic fit to $\sigma^{\circ}_{surf}$ in log-log space compared to the non-parametric fit.


[2] S. Lehner, J. Horstmann, W. Koch, and W. Rosenthal, "Mesoscale wind measurements using recalibrated ERS SAR images," *Journal of Geophysical Research*, vol. 103, pp. 7847–7856, 1998.

[3] R. K. Raney, A. P. Luscombe, E. J. Langham, and S. Ahmed, "RADARSAT," in *Proc. IEEE International Geoscience and Remote Sensing Symposium*, 1991, pp. 839–849.

[4] C. Melsheimer, W. Alpers, and M. Gade, "Simultaneous observations of rain cells over the ocean by the synthetic aperture radar aboard the ERS satellites and by surface-based weather radars," *Journal of Geophysical Research*, vol. 106, no. C3, pp. 4665–4677, 2001.

[5] D. Atlas, "Footprints of storms on the sea: A view from spaceborne synthetic aperture radar," *Journal of Geophysical Research*, vol. 99, pp. 7961–7969, 1994.

[6] C. Nie and D. G. Long, "A C-band wind/rain backscatter model," *IEEE Trans. Geosci. Remote Sens.*, vol. 45, no. 3, pp. 621–631, 2007.

[7] D. R. Thompson, T. M. Elfouhaily, and B. Chapron, "Polarization ratio from microwave backscattering from the ocean surface at low to moderate incidence angles," in *Proc. IEEE International Geoscience and Remote Sensing Symposium*, Seattle, WA, 1998.

[8] T. Elfouhaily, "Physical modeling of electromagnetic backscatter from the ocean surface; application to retrieval of wind fields and wind stress by remote sensing of the marine atmospheric boundary layer," Ph.D. dissertation, IFREMER, Plouzane, France, 1997.

[9] J. Gower and S. Skey, "Wind, slick, and fishing boat observations with RADARSAT ScanSAR," *Johns Hopkins APL Technical Digest*, vol. 21, no. 1, 2000.

[10] J. Hallet and L. Christensen, "Splash and penetration of drops in water," *J. Rech. Atmos.*, vol. 18, pp. 225–242, 1984.

[11] L. J. Battan, *Radar observation of the atmosphere*. The University of Chicago Press, 1973.

[12] C. Nie, *Wind/Rain Backscatter Modeling and Wind/Rain Retrieval for Scatterometer and Synthetic Aperture Radar*, Ph.D. Dissertation, Brigham Young University, 2008.